Additive Manufacturing 12 (2016) 16–24

Contents lists available at ScienceDirect

Additive Manufacturing

journal homepage: www.elsevier.com/locate/addma

MRI monitoring and non-destructive quality measurement of polymeric patterns manufactured via stereolithography

Evgeny V. Morozov[a,b,*], Mikhail M. Novikov[c], Vyacheslav M. Bouznik[d]

[a] Kirensky Institute of Physics SB RAS, Krasnoyarsk, Russia
[b] Institute of Chemistry and Chemical Technology SB RAS, Krasnoyarsk, Russia
[c] Institute on Laser and Information Technologies RAS, Shatura, Russia
[d] All-Russian Scientific Research Institute of Aviation Materials, Moscow, Russia

ARTICLE INFO

Article history:
Received 22 November 2015
Received in revised form 28 April 2016
Accepted 10 May 2016
Available online 24 May 2016

Keywords:
MRI
Stereolithography
Polymers
Build parameters
Aging

ABSTRACT

The use of Magnetic Resonance Imaging (MRI) for monitoring, studying and performing output quality measurements of the acrylate-based polymeric patterns manufactured using stereolithography (SL) was introduced in this work. The effects of build parameters and humid environment on sample homogeneity, distribution of crosslink density, stability and defect formation were examined. The spatial resolution of the method was found to be sufficient to identify patterns according to the build parameters used and to detect specific hatch-predicted crosslink density variations. Qualitative information obtained using MRI visualisation was supplemented by quantitative measurements of Nuclear Magnetic Resonance (NMR) relaxation times and ^{1}H NMR spectra. NMR spectroscopy confirmed the identity of the chemical composition among the patterns and showed that the crosslink density variation observed via spatially resolved T_2-profiles stems from the difference of the build parameters. Different types of defects in the samples were observed and classified; some defects originated from local matrix continuity failures (partially cured resin trapping within the polymer or bubbles formation), while other defects were found in the form of bulk layering. MRI visualisation coupled with relaxometry and ^{1}H spectroscopy of patterns during their interaction with humidity allowed tracking water distribution inside the sample and observing effects of swelling, fracturing and chemical decomposition. It was found that the initial inhomogeneous structure of the specimen has a crucial role in subsequent fracturing due to non-uniform expansion of the swollen parts. As a result, the approach presented in this work improves the output quality control and current testing techniques, provides insight how physical properties of the 3D parts are affected by different technical parameters, and eventually can help the use of SL technologies for a variety of applications.

1. Introduction

Additive manufacturing (AM) is a rapidly growing innovative technology that is being incorporated into a broad range of applications in diverse areas, such as industry, medicine, materials science, education, and art. The first technique that can be referred to as AM was introduced in the 1980s [1]. Since then, a large number of competing technologies have been developed, involving such processes as binder jetting, directed energy deposition, material extrusion, material jetting, powder bed fusion, sheet lamination, and vat photopolymerisation [2]. Among these technologies, stereolithography (SL, which based on the vat photopolymerisation) is one of the most widely used around the world [3]. SL allows the fabrication of parts with complex geometries and surface finishes comparable to many conventionally machined components. This technology utilizes a laser beam to selectively draw or print cross-sections of a model on a photocurable resin surface. This action is repeated on the surface of the resin in a layer-by layer method until a 3D part is created.

Active incorporation of AM technologies into industrial applications imposes requirements on the 3D parts created. The mechanical properties (such as toughness, elasticity, tensile stress), heat resistance, durability, homogeneity, surface finish, and stability play a crucial role when substituting parts in machines or structures with those manufactured using the SL process. It becomes even more pronounced in cases when 3D parts are to be used under significant loading and/or in an aggressive envi-

* Corresponding author at: Kirensky Institute of Physics SB RAS, Akademgorodok 50/38, 660036 Krasnoyarsk, Russia.
E-mail addresses: emorozov@kth.se, morozov_if@mail.ru (E.V. Morozov).

http://dx.doi.org/10.1016/j.addma.2016.05.015
2214-8604/

ronment. There are several important factors that can contribute to the physical properties exhibited in parts created using the SL process and their stability: build parameters and build orientation, post-curing process, addition of reinforcing material to the resin, aging and environmental conditions [4–7]. Many research studies are investigating these factors with the goal of improving the overall properties of SL-manufactured parts. However, majority of the studies presented in the literature have mainly dealt with the effects of the factors on the mechanical properties of the finished parts. For example, the tensile stress and modulus of elasticity of SL-manufactured parts were tested depending on orientation of patterns (i.e., whether a sample was built flat or on an edge) [8–10]. Typically, mechanical testing of the manufactured part results in irreversible destruction of the sample, making it no longer affordable for any subsequent investigation. Traditional destructive techniques also fail to give accurate information regarding influence of technical parameters on polymer crosslink density variations, possible defects occurring inside the patterns and their eventual stability. Constantly growing demand for AM parts requires comprehensive investigation of them, including non-destructive methods [11]. They can provide internal samples features such as homogeneity, distribution of polymer crosslink density, presence of defects and their origin, etc.

Magnetic Resonance Imaging (MRI) is a well-known advanced method that provides non-destructive visualisation of non-metallic samples, their internal structure and the various processes occurring within them [12]. MRI was first developed for medical applications but is now actively used and integrated into chemical engineering and materials science [13]. Polymers, composites, catalysts and other advanced materials, processes of polymerisation, hardening, heat and mass transport have been successfully studied by MRI. Nevertheless, until now, the implementation of MRI in additive manufacturing has focused primarily on the biomedical applications; for example, based on Nuclear Magnetic Resonance (NMR) images of tissues and structures, the digital prototypes were reconstructed by the subsequent 3D printing of the appropriate parts [14–17]. In one work [18], a special controllable phantom intended to substitute the real bone tissues was fabricated via SL and then it was used for MRI investigation of pore geometry. In that work authors just simplified the structure under investigation by preparing stereolithographic samples with controlled structural elements whereas no attempts to investigate the quality of the samples were done there. In result, the SL manufactured parts have never been studied by MRI to examine the influence of common AM parameters on the output quality and stability of final samples. MRI can be applied for non-destructive visualisation of polymer crosslink density distribution with the aim to correlate intrinsic sample features with technical parameters as well as with its following behaviour in aggressive chemical environment. Absorption mechanisms, moisture uptake pathways, internal swelling during humidity aging can be easily investigated by MRI as well. Such MRI studies may sufficiently improve our understanding of the role of the different factors (such as technical parameters, resin composition, polymer crosslink density distribution, homogeneity, defects, aging conditions etc.) on the overall properties of SL-manufactured parts.

To examine the feasibility of the method, a complex approach involving MRI, NMR relaxometry and NMR spectroscopy was applied in the research presented here for the first time for the monitoring and non-destructive quality measurement of 3D patterns manufactured using the SL process. In contrast to previous studies carried out by conventional methods, MRI focuses on visualisation of polymer crosslink density distribution within the patterns with the aim to observe possible inhomogeneities and defects occurring during the light induced curing processes and aging. In result, such approach is supposed to identify the role of hatch, build parameters and resin composition in samples stability related with particular type of defects. Taking into account that environmental conditions impact the stability and fracture formation in the samples, the humidity effect on the patterns was also examined via MRI.

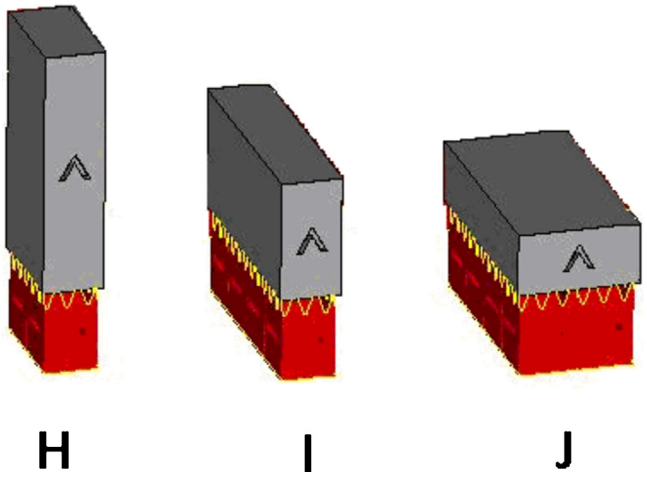

Fig. 1. Scheme of patterns printed on the platform in three different orientations (layouts H–J as described in Section 2.1); the supports are presented in red colour. The checkmarks on the sample's side point out the direction of growth during manufacturing. (For interpretation of the references to colour in this figure legend, the reader is referred to the web version of this article.)

2. Materials and methods

2.1. Samples and equipment

A set of polymer parallelepiped patterns was manufactured in three different orientations: either flat or on an edge relative to the *x-y* plane, referred to as layouts H, I and J, where H refers to samples with the layers stacked across the length (20 mm), I refers to samples with the layers stacked across the width (10 mm), and J refers to samples with the layers stacked across the thickness (5 mm) of the sample, Fig. 1. Patterns were also labelled according to hatch used during their manufacturing: batch 1–xy-linear (0.2 mm hatch spacing), batch 2–the same xy-linear with an offset loops formed by equidistant to the main circuit (1 mm offset loops thickness) and batch 3–spiral (0.2 mm hatch spacing, 10 mm distance between the centres), Fig. 2. Every specimen was printed out with 4–5 replicates.

For pattern manufacturing different photopolymer compositions were used, including those prepared in our laboratory as well as commercially available. Home-made resins were IPLIT3 and R405 with the following components: oligo glycerolmethacrylate, 2,2-bis(*n*-3-methacryloyloxy 2-hydroxypropoxy 4-phenyl)propane, bis(methacryloyl)oligo(triethylene glycol)phthalate, photoinitiator IRGACURE 651; in case of R405 the oligo urethane methacrylate and photosensitiser (Michler's ketone) were added for resin modification and plasticizing. All components were purchased from Sigma-Aldrich. Commercial resin used was epoxy-based ProtoTherm 12120 (DSM Somos®Materials) with the following components: trimethilolpropane diglycidylether bis-(epoxycyclohexyl)-methylcarboxylate, bisphenol-*A*-(epichlorhydrin) epoxyresin reaction product, 3-ethyloxetane 3-methanol formaldehyde reaction product with 1-chloro-2,3-epoxypropane/phenol, 7-oxabicyclo hept-3-ylmethyl 7-oxabicyclo heptane-3-carboxylate propylene carbonate.

The patterns were printed using our own SL apparatus equipped with different commercial lasers. They were quasi-CW DPSS laser model 3505 (DPSS Inc., USA) with a laser wavelength of 355 nm,

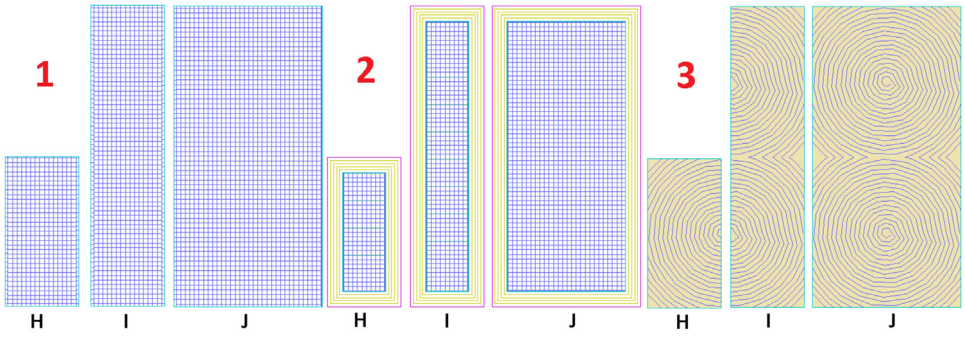

Fig. 2. Scheme of three types of hatches used during patterns manufacturing: 1-xy-linear, 2-xy-linear with offset loops formed by equidistant to the main circuit, and 3-spiral. H–J notations correspond to layouts.

beam diameter of 0.4 mm and output power of 120 mW; CW Blue Purple semiconductor laser model GS-405D200mw (DPSS Inc., USA) with a laser wavelength of 405 nm, beam diameter of 0.4 mm and output power of 40 mW; CW He-Cd laser model GKKL-30UM (Plazma Ltd., Russia) with a laser wavelength of 325 nm, beam diameter of 0.2 mm and output power of 20 mW. To address some issues emerged during patterns investigation, number of samples were also printed out using DLP method (DLP apparatus "B9Creator" v.1.2, B9Creations LLC USA, resins are B9R-1-Red and B9R-1-Cherry, US Composites Inc.).

To avoid the influence of the platform roughness on the pattern geometry, the supports consisted of the cured polymer layers with higher density printed first (6–7-mm thickness, supports are presented in Fig. 1). Variation of polymer crosslink density was attained by changing the exposure time of the laser beam, whereas its output power was kept constant.

2.2. MRI method

MRI experiments were performed using an installation based on a Bruker AVANCE DPX 200 console and superconducting magnet with an 89-mm diameter vertical bore, water-cooled and self-shielded Bruker gradient set (maximum gradient strength up to 1 T/m); probe PH MICRO 2.5, 25-mm internal diameter birdcage coil tuned and matched to ^{1}H nuclear resonance frequency of 200.13 MHz; and a console operated with Paravision 4.0 software. Acquisition of ^{1}H NMR spectra and measurements of T_2 relaxation time were performed using the same equipment and probe configuration. The weight measurements were performed using an analytical balance GH-252 manufactured by A&D, Japan.

The principles of the MRI technique are well known and are not presented here in detail (the basic information regarding the operational principles of MRI can be found in [12,13,19]). In general, the MRI approach allows for measuring of the intensity of the NMR signal that comes from the selected area of the sample. In fact, using MRI, one can achieve a 2D map of the NMR signal intensity distribution that, in turn, is strongly correlated with local relaxation times T_1 and T_2. The relaxation time depends on different parameters of the system (polymer matrix density, chemical composition, magnetic susceptibility, diffusion coefficient and many others) because these parameters can change the correlation time of the fluctuating local magnetic field. According to Bloembergen-Purcell-Pound theory, the T_2 relaxation time decreases as the correlation time increases [20]; thus, if a particular part on the T_2-weighted NMR image demonstrates lower signal intensity compared to the other parts of the sample, then this particular region definitely belongs to samples part with longer correlation times, i.e., the part with higher crosslink density and/or relatively immobile molecules. For example, this effect is easily visualised on NMR images of polymer materials, where parts with higher crosslink density of polymer network appear with lower signal intensity [12]. For convenience, extent of polymerization (polymer crosslink density) in this work was referred to as simply "density" unless otherwise mentioned.

2D NMR images were acquired using the standard pulse sequences supplied by the imager software: R405-based samples with relatively higher relaxation times were studied with Gradient Echo Fast Imaging (GEFI) technique while all other samples having demonstrated lower relaxation times were studied with the most suitable Single Point Imaging (SPI) technique [21]. Quantitative T_2-profiles were evaluated by plotting T_2 vs. the coordinate corresponding to the position of the pixel on the T_2-map (special T_2-maps were plotted by the processing of image sequences acquired via the Multi Slice Multi Echo technique and are not presented in the work). For GEFI technique the parameters of image acquisition were following: slice thickness of 0.5 mm; field of view (FOV) of 40 mm; matrices of 128 × 128 pixels; repetition time (TR) = 100 ms, echo time (TE) = 1.8 ms, number of scans = 100, image acquisition time = 21 min. For SPI technique the images were acquired without slice selection i.e. the virtual slice thickness is bigger than the real thickness of the sample; all other parameters were following: FOV of 40 mm; matrices of 64 × 64 pixels; TR = 4 ms, dephasing time = 0.1 ms, number of scans = 10, image acquisition time = 3 min.

After manufacturing, all of the specimens were stored in a sealed pack at room temperature to avoid the impact of air humidity. During the MRI experiment, the sample was placed in a glass tube (12-mm inner diameter): this tube was inserted into the MRI probe, and the image acquisition process was started immediately. A temperature of 25 ± 1 °C was maintaining during the measurement. To study the effect of humidity on SL manufactured patterns, prior to the MRI measurements, the specimens were exposed in distilled water (at 25 °C) for different periods of time. Every MRI measurement was accompanied by the acquisition of bulk ^{1}H NMR spectra of samples and their weighing.

3. Results and discussion

3.1. Output quality measurement

MRI visualisation of the R405-based specimens manufactured in flat orientation (layout J) revealed different character of signal intensity distribution, depending on the hatch used. Patterns with an xy-linear hatch were found to be homogeneous within the every slice visualised, Fig. 3a. Small thickness of the layers formed during light-induced curing (0.2 mm) is at the limit of the method resolution, but some net-like structure of the image can be observed. A homogeneous signal distribution corresponds to the uniform distribution of the polymer density all over the sample, i.e., uncured or partially cured resin has not been trapped within the photopolymer during fabrication. Imposition of additional offset loops to the main circuit is expected to yield offset layers with higher density. In addi-

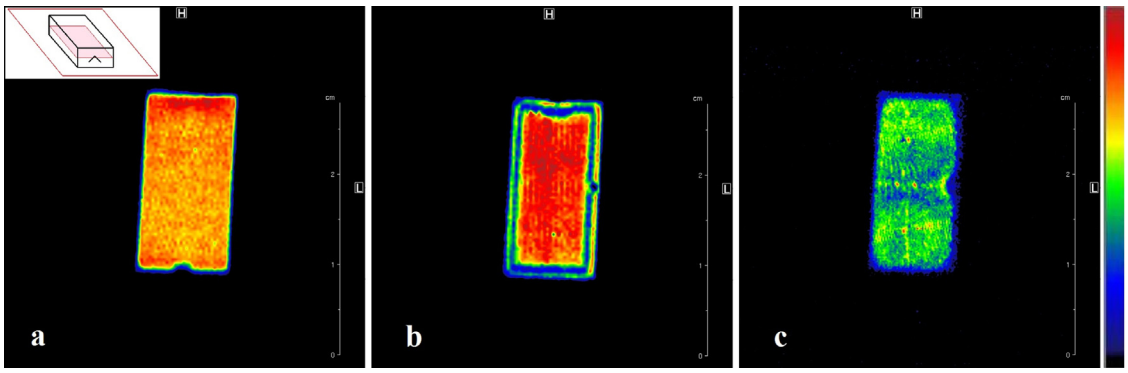

Fig. 3. NMR images of central transverse slice of the R405-based patterns in layout J; batch 1 (a), 2 (b) and 3 (c); the geometry of the slice planes is the same for all images and is schematically presented on the first of them. Colour bar corresponds to NMR signal on the images; higher value of the signal (red and yellow colours) implies lower crosslink density while the lower value of the signal (green and blue colours) implies higher density. (For interpretation of the references to colour in this figure legend, the reader is referred to the web version of this article.)

tion, it was actually observed on the NMR images: every slice of the sample demonstrates the edges with low signal intensity, Fig. 3b. Note that inside the edges of the specimen, the polymer density distribution is uniform. Unlike these cases, MRI visualisation of the samples with a spiral hatch revealed a rather inhomogeneous density distribution. One can evidently observe that the NMR image of this pattern contains two concentric regions in the positions predicted by the hatch geometry; the distance between the centres of the regions is approximately 10 mm, Fig. 3c. Within every circuit, the density distribution can be considered homogeneous, but their junction is the source of eventual defects due to breaking of continuity. The spatial resolution of SPI technique was found to be insufficient to visualize the hatch used in IPLIT3- and ProtoTherm-based specimens since this technique does not allow using slice selection. Therefore SPI visualisation was applied there for detecting of crosslink density distribution, possible defects and aging of patterns regardless the type of hatch.

While NMR images provide only qualitative information about the homogeneity and the distribution of the polymer crosslink density within the every specimen, spatially resolved measurements of the T_2 relaxation times give quantitative information about the crosslink density itself and allow for comparison between the samples. Thus, T_2 profiles plotted across the length of the R405-based samples (along the width in slice plane presented in Fig. 3) revealed that the photopolymer densities are slightly different for pattern batches 1, 2 and 3, Fig. 4a. Compared to the xy-linear hatch, offset loops visualised with lower signal intensity indeed were found to have the lowest T_2 values. The relaxation time values inside the circuit there, though, are higher than those in batch 1. Creating of the dense layers on the edges causes the internal layers to be cured with slightly lower degree of polymerization to avoid substantial strain due to sample shrinkage. Pattern batch 3 demonstrates the lower T_2 values compared to patterns with the xy-linear hatch. The steady and uniform spiral manner of curing yields a higher density of polymer in the sample layers.

As described in Section 2.2, in addition to the relaxation times being affected by the density of the polymer matrix, the chemical composition can also contribute to the eventual T_2 values. To check this effect, the ^{1}H NMR spectra of the bulk R405-based samples were recorded at the same time. The spectra of all specimens were found to be very similar and contain three different groups of protons with mean chemical shifts of 7.45 ppm (aromatics), 3.67 ppm (protons associated with carbonyl, carboxyl, ether groups) and 1.25 ppm (methylene groups), Fig. 4b. Due to strong dipole–dipole interaction of the relatively immobile protons (dynamic of the polymer chains is substantially restricted despite of their residual flexibility), all of the lines in the spectrum are broadened and overlapping. Nevertheless, this spectrum is recognizable and well consistent with the spectra of typical acrylate polymers presented in the literature [22,23]. In fact, the effects described above are due to the density variations that appeared during light-induced curing, and the chemical composition changes are negligible.

In addition to studying the factors affecting on density distribution, one of the most important applications of MRI visualisation of the SL-manufactured patterns is non-destructive output quality measurement. It was previously determined that the build orientation is affecting the mechanical properties of the specimens: the adhesion of the material between successive layers is generally weaker than the adhesion between material within a layer, and the orientation of the part in the build chamber affects the number of layers used to manufacture the part [7]. NMR images of the R405-based patterns built in different orientations (layout H and I) revealed their strong inhomogeneity, Fig. 5. The vertically built patterns consisted of three different bulk layers of polymer: the first one (top of the sample) had the highest density, followed by the second (intermediate) and the third (bottom part of the specimen) layers with lower densities, Fig. 5a. Every layer was found to have a sharp interface; in some cases, the interfaces were visualised with high signal intensity, indicating that the partially cured resin has been trapped between the bulk layers during fabrication. NMR images of patterns built on the edge (layout I), however, visualised only two bulk layers unlike patterns H described, Fig. 5b. Evidently, these two layers appeared during manufacturing in the same way as those found in a bottom part of pattern H: these layers have similar width, T_2 values and density. The third layer was not shown here only due to the sample's smaller width; the polymer with the highest density likely would appear if the sample width could exceed 10 mm.

Thorough investigation of misbehaviour found in layouts H and I revealed that the actual reason was the laser stability failures during manufacturing: output power of the laser was slightly increasing that resulted in higher extent of polymerization in the end of printing process. Using of different laser sources however revealed another defect of manufacturing. According to the technical procedure, the crosslink density along the sample length should be slightly increased towards the bottom of the specimens because the laser beam is partially passing through the current layer, causing the underlying layers to be slightly over cured. It was experimentally found in IPLIT3-based patterns, Fig. 5c. One can see that there are no interfaces and crosslink density distribution is smooth. This effect has been previously examined in the works [24,25], where it was shown that the total energy absorbed by photopolymer increases when more layers are built. MRI visualisation of the epoxy-based specimens and those manufactured

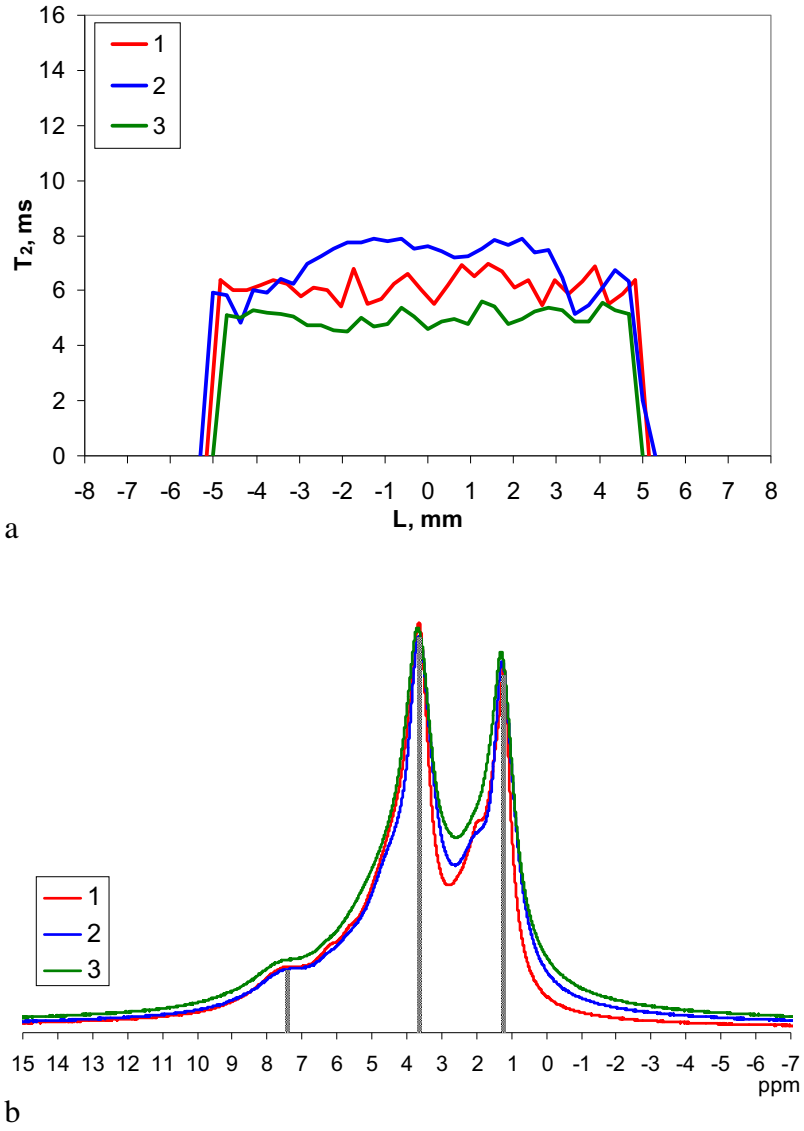

Fig. 4. Series of T_2 profiles along the width of the samples (a) and ^1H NMR spectra (b) of R405-based patterns, notations of 1, 2 and 3 are the corresponding batches; all of the data are presented for layout J.

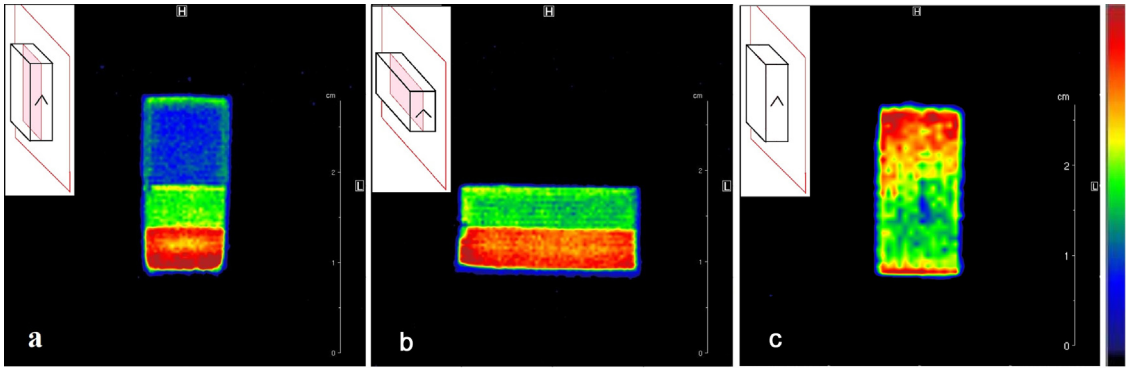

Fig. 5. NMR images of the central transverse slice, demonstrating examples of strong inhomogeneities associated with build orientation; R405-based (a, b) and IPLIT3-based (c) patterns, all of them are from batch 1, layouts H (a, c) and I (b); the geometries of slice planes are schematically presented on the images. Colour bar corresponds to NMR signal on the images; higher value of the signal (red and yellow colours) implies lower crosslink density while the lower value of the signal (green and blue colours) implies higher density. (For interpretation of the references to colour in this figure legend, the reader is referred to the web version of this article.)

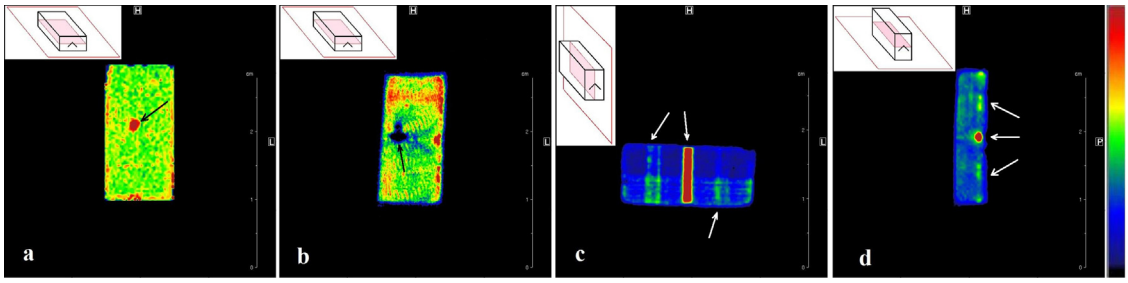

Fig. 6. NMR images of transverse slice of R405-based patterns, demonstrating examples of defects; pattern batches 1 (a) and 3 (b–d); layouts J (a, b) and I (c, d); the geometries of slice planes are schematically presented on the images. Defects referenced in the text are depicted by arrows.

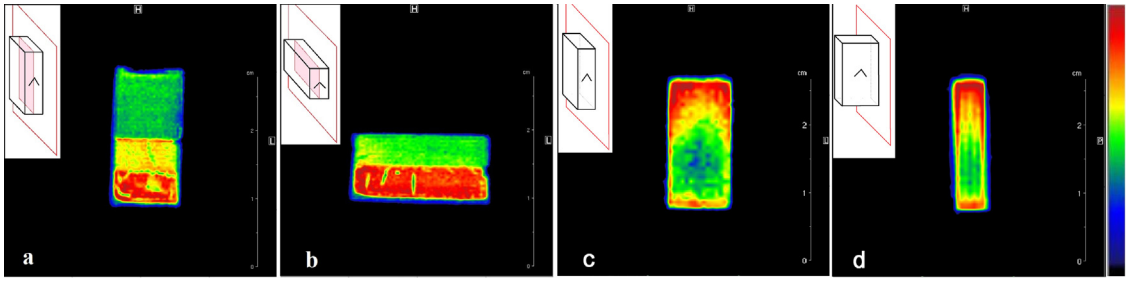

Fig. 7. NMR images of R405-based (a, b) and IPLIT3-based (c, d) patterns during patterns – humidity interaction; all of them are from the batch 1, layouts H (a, c, d) and I (b). Time of soaking is 24 days. The geometries of the slice planes are schematically presented on the images.

via DLP method (used as a reference) revealed high quality of the patterns with homogeneous density distribution.

MRI method is capable of visualising the different types of defects that occur during SL manufacturing. For example, partially cured resin trapped within the photopolymer can be visualised in the bulk (Fig. 6a). The series of defects caused by features of the hatch were found in the patterns. As mentioned above, breaking of the continuity in the circuits' junction (R405-based patterns, batch 3) becomes the source of the defects: gaps and bubbles were often found in that area (Fig. 6b). One more type of defect associated with the spiral hatch was observed: centres of the circuits and their junction sometimes appear partially cured (Fig. 6c and d). MRI non-destructive quality measurement allows either selection of non-defective patterns or clarification of the influence of the build orientation/hatch on the homogeneity and the polymer density.

3.2. MRI monitoring of humid environment effects on the patterns

The effect of humidity on the SL manufactured parts can be associated with different processes, such as moisture uptake, swelling, chemical decomposition of polymer matrix and cracks formation. NMR images of the patterns exposed to distilled water at room temperature revealed a homogeneous distribution of absorbed water over the samples, regardless of the time of exposure. In cases where the initial pattern was inhomogeneous and comprised the layers with different density of polymer, the wet sample retains that layered structure, Fig. 7. Evidently, water uptake sufficiently changes the physical properties of the polymer, leading to uncompensated stress and internal fracturing. Indeed, MRI revealed the formation of intensive cracks in the specimens, but the majority of the cracks appeared in layers with the lowest polymer density (Fig. 7, R405-based specimens). In contrast, the layers with higher density in R405-based samples as well as IPLIT3- and epoxy-based patterns are quite stable. This effect is most likely caused by non-uniform swelling: the polymer network with lower crosslink density is prone to swelling to a higher extent than that with a higher density, resulting in a non-uniform increase of the sample dimensions, shear stress and deformation. This effect observed via MRI is in agreement with previously presented data for the acrylate-based SL-manufactured parts [6]: specimens with lower density revealed much stronger water absorption, swelling and shape distortion effects.

In cases where the initial pattern was homogeneous, the wet sample is stable to cracks because the swelling processes result in isotropic dimensions expansion. For example, NMR images of patterns belonged to R405-based patterns (batch 2) with the offset loops demonstrating large cracks, whereas the images of the other patterns show only minor effects, Fig. 8. For the same reason, the bulk T_2 measurements of the patterns demonstrate steady growth of T_2 values with time of exposure for batch 2, whereas relaxation times for batches 1 and 3 reach the plateau, Fig. 9a. Note that water-induced growth of the relaxation time in the patterns is a result of two different processes: increasing of water content itself (water molecules are moving fast and have a very long T_2) and increasing of mobility of polymer chains due to partial density loss induced by swelling. As observed (Fig. 9a), both swelling and water absorption processes approach equilibrium, which is determined by the nature of the polymer, except the specimens in batch 2, where absorption is more intensive due to the large cracks.

Dynamics of the relaxation times and the difference between pattern batches were well confirmed by weight measurements. Water absorption and growth of weight were observed during the first 10 days of exposure to water, but after that time, the weight of the samples began to decrease, Fig. 9b. This effect was explained by the partial decomposition of polymer and the dissolving of its constituents in water. Despite the decomposition followed by loss of mass, the relaxation times reflect the dynamics of the residual sample; therefore, there is no effect of decreasing similar to that found in the weight measurements.

Partial decomposition followed by subsequent dissolving of the polymer in water was examined using ^{1}H NMR spectroscopy. NMR spectra recorded during water uptake demonstrate the initial increase of the intensity of the central peak and the formation of a "shoulder" corresponding to absorbed water (chemical shift of water peak is approximately 4.7 ppm), Fig. 10a. However, the

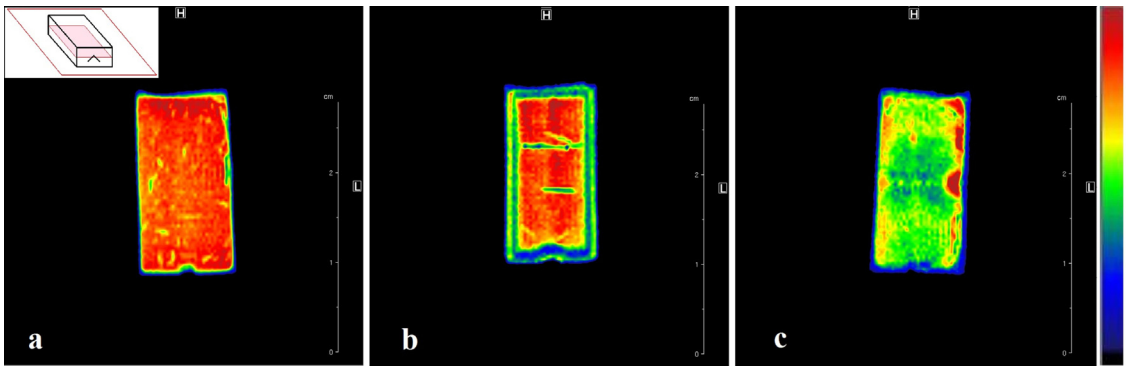

Fig. 8. NMR images of central transverse slices demonstrating different behaviour of R405-based patterns, depending on the hatch and initial homogeneity during patterns – humidity interaction; pattern batches 1 (a), 2 (b) and 3 (c) after 24 days of exposure to distilled water; layout J. The geometry of the slice plane is the same for all images and is schematically presented on the first of them.

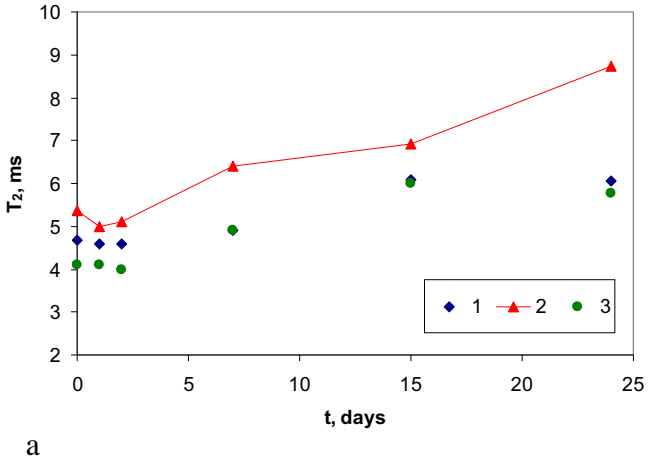

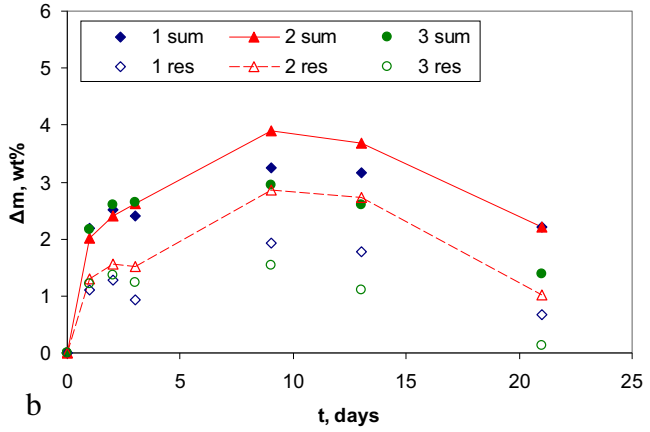

Fig. 9. T_2 relaxation times (a) and weight (b) changes with time of exposure to distilled water; the weight of the samples was measured twice: the first time – 10 min after samples removal from container with water (index "sum") and then 3 h later (index "res") to fix the residual samples weight after partial water evaporation.

spectrum of a long-time soaked sample shows a lower intensity of central peak, while the other peaks corresponded to aromatic and methylene protons that exhibit approximately the same intensities (intensity of water peak is increasing). Thus, only the peak of oxygen-coupled protons was affected by water, and it may be the result of partial hydrolysis of the ether groups.

As mentioned above, swelling of the polymer matrix leads to an increase of the sample dimensions; this expansion is isotropic for initially homogeneous specimens. T_2 profiles evaluated during this process revealed steady and uniform growth of the relaxation times, accompanied with a small increase of the sample width (up to ~10%), Fig. 10b.

The results demonstrating the influence of build parameters and humid environment on SL-manufactured patterns described in the current work are consistent with the data presented in previous works, where researchers dealt with the testing of physical properties of the AM parts depending on the materials used, build parameters, aging, and environment conditions. In works [8,9], the tensile strength was measured for specimens manufactured in different orientations and variation of parameter was found within 5–13%. The differences found in ultimate tensile strength and modulus of elasticity were 3.5 and 4.6%, respectively, between samples built flat or on an edge [10]. The differences found could have been caused by the similar type of defects as those observed by MRI in the current article. For additively manufactured parts, mechanical properties are generally anisotropic due to the layer-based manufacturing process. Therefore, any failures during the formation of the layers may result in a significant effect. As concerning the effects of humidity on the mechanical properties of SL manufactured parts observed in the works of [4,6,7], MRI results are considered to be consistent, providing deep insight into the role of inhomogeneities on water absorption, swelling and eventual fracturing. It is worth to emphasize, the effects of the build parameters and humid environment on the properties of AM parts have a general nature and they were also studied for other AM technologies [26,27].

4. Conclusions

The present work introduced an MRI-based approach for monitoring, studying and performing output quality measurements of the polymeric patterns manufactured using stereolithography. MRI non-destructive visualisation of the patterns revealed the strong influence of the build orientation (layout), hatch, laser stability, resin composition on sample homogeneity, distribution of crosslink density and defect formation. In particular, the spatial resolution of the NMR images was found to be sufficient to allow for identifying the xy-linear or spiral hatch in samples with relatively high relaxation times. In addition, specific hatch-predicted crosslink density variations were also detected. Using of the NMR relaxometry with high spatial resolution significantly improved the capabilities of the MRI method, giving quantitative information about samples density and allowing for comparison of the different batches of patterns. Thus, the patterns with spiral hatch were found to be the densest. ^{1}H NMR spectroscopy applied at the same time confirmed the identity of the chemical composition among the patterns; any density variations were observed to come from the hatch or the lay-

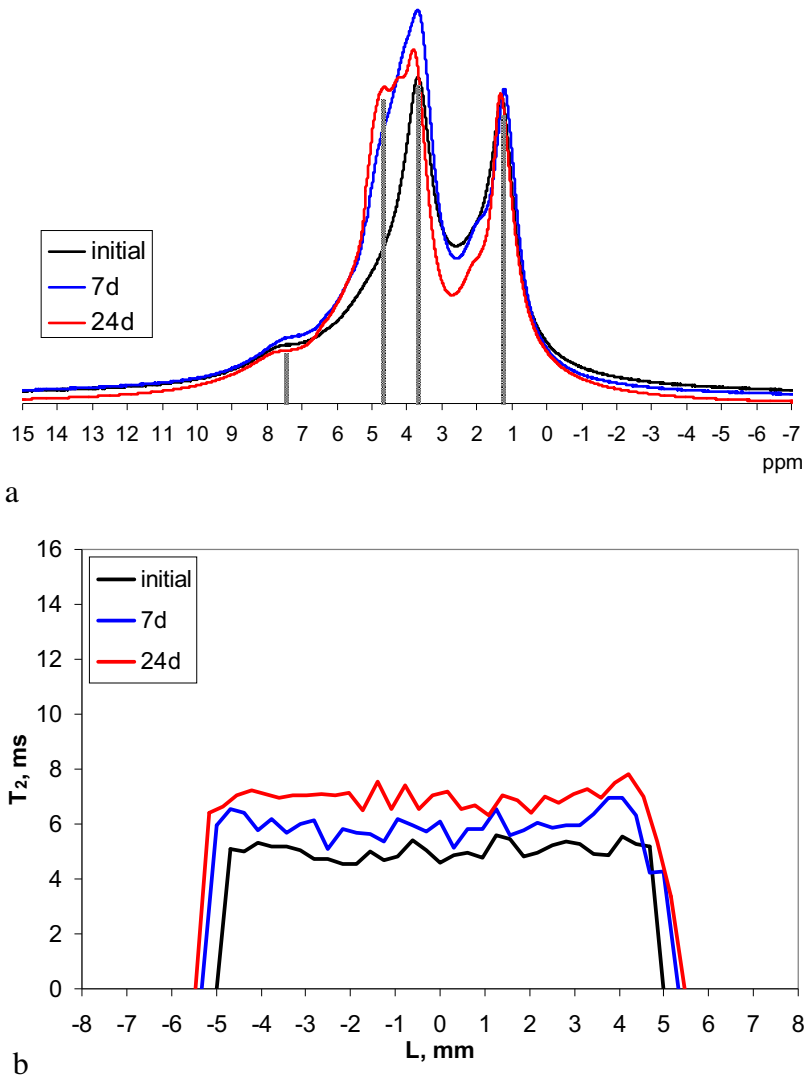

Fig. 10. ^{1}H NMR spectra (a) and series of T_2 profiles along the samples width (b) during R405-based pattern – humidity interaction; the results are presented for patterns batch 3, layout J.

out used. Different types of defects in the samples were observed and classified; some of these defects originated from the local matrix continuity failures (partially cured resin trapping within the polymer or bubbles formation), whereas other types of defects were found in the form of bulk layering.

MRI visualisation coupled with relaxometry and ^{1}H spectroscopy of patterns during their interaction with humidity allows for tracking of the water distribution inside the sample and observing the effects of swelling, fracturing and chemical decomposition. NMR images showed that the initial inhomogeneous structure of the specimen plays a crucial role in subsequent fracturing due to non-uniform expansion of the swollen parts. At the same time, the specimens that have a homogeneous density distribution (and contain no defects) are only slightly affected by humidity, regardless of the hatch. The NMR relaxation and spectral data were correlated with weight measurements, and their analysis revealed the effect of partial chemical decomposition followed by dissolving of the constituents. The impact of the build orientation, hatch, and humid environment examined in this work correlates well with the data presented in the literature.

The results show that the MRI approach proved to be an efficient tool for studying SL manufactured parts, and this method can be successfully used to complement the standard mechanical testing that is currently widely used. In a practical sense, the approach presented in our work is relevant and can help the use of SL technologies for a variety of applications. Non-destructive monitoring may assist in improving the output quality control for those who are developing current testing techniques; it may give insight into how the physical properties of the 3D parts are affected by different technical parameters.

Acknowledgements

This research was performed with the financial support of Russian Foundation for Basic Research (project no. 14-29-10178 ofi_m).

References

[1] P. Jacobs, Stereolithography and Other RP&M Technologies: From Rapid Prototyping to Rapid Tooling, ASME Press, New York, 1996.
[2] I. Campbell, D. Bourell, I. Gibson, Additive manufacturing: rapid prototyping comes of age, Rapid Prototyp. J. 18 (2012) 255–258.
[3] C. Yi, L. Dichen, W. Jing, Using variable beam spot scanning to improve the efficiency of stereolithography process, Rapid Prototyp. J. 19 (2013) 100–110.
[4] X. Ottemer, J.S. Colton, Effects of aging on epoxy-based rapid tooling materials, Rapid Prototyp. J. 8 (2002) 215–223.

[5] K. Chockalingam, N. Jawahar, U. Chandrasekhar, Influence of layer thickness on mechanical properties in stereolithography, Rapid Prototyp. J. 12 (2006) 106–113.
[6] C. Tröger, A.T. Bens, G. Bermes, R. Klemmer, J. Lenz, S. Irsen, Ageing of acrylate-based resins for stereolithography: thermal and humidity ageing behaviour studies, Rapid Prototyp. J. 14 (2008) 305–317.
[7] K. Puebla, K. Arcaute, R. Quintana, R.B. Wicker, Effects of environmental conditions, aging, and build orientations on the mechanical properties of ASTM type I specimens manufactured via stereolithography, Rapid Prototyp. J. 18 (2012) 374–388.
[8] R. Hague, S. Mansour, R. Saleh, R. Harris, Materials analysis of stereolithography resins for use in rapid manufacturing, J. Mater. Sci. 39 (2004) 2457–2464.
[9] J.M. Dulieu-Barton, M.C. Fulton, Mechanical properties of a typical stereolithography resin, Strain 36 (2000) 81–87.
[10] R. Quintana, K. Puebla, R.B. Wicker, Effects of build orientation on tensile strength for stereolithography manufactured ASTM D-638 type I specimens of DSM Somos 11120 resin, J. Adv. Manuf. Technol. 46 (2010) 201–215.
[11] M. Gatto, R.A. Harris, Non-destructive analysis (NDA) of external and internal structures in 3DP, Rapid Prototyp. J. 17 (2011) 128–137.
[12] B. Blumich, NMR Imaging of Materials, Clarendon Press, Oxford, 2003.
[13] S. Stapf, S.-I. Han, NMR Imaging in Chemical Engineering, WILEY-VCH, Weinheim, 2006.
[14] S. Swann, Integration of MRI and stereolithography to build medical models: a case study, Rapid Prototyp. J. 2 (1996) 41–46.
[15] G. Undt, K. Wild, G. Reuther, R. Ewers, MRI-based stereolithographic models of the temporomandibular joint: technical innovation, J. Cranio Maxillofac. Surg. 28 (2000) 258–263.
[16] G.F. Greil, I. Wolf, A. Kuettner, M. Fenchel, S. Miller, P. Martirosian, et al., Stereolithographic reproduction of complex cardiac morphology based on high spatial resolution imaging, Clin. Res. Cardiol. 96 (2007) 176–185.
[17] F. Rengier, A. Mehndiratta, H. von Tengg-Kobligk, C.M. Zechmann, R. Unterhinninghofen, H.-U. Kauczor, F.L. Giesel, 3D printing based on imaging data: review of medical applications, Int. J. CARS 5 (2010) 335–341.
[18] B. Issa, P. Gibbs, R. Hodgskinson, C.M. Langton, L.W. Turnbull, Assessment of the pore geometry of stereolithographic models by high resolution MRI, Magn. Reson. Imaging 16 (1998) 651–653.
[19] P. Callaghan, Principles of Nuclear Magnetic Resonance Microscopy, Clarendon Press, Oxford, 1993.
[20] N. Bloembergen, E.M. Purcell, R.V. Pound, Relaxation effects in nuclear magnetic resonance absorption, Phys. Rev. 73 (1948) 679.
[21] M.A. Bernstein, K.F. King, X.J. Zhou, Handbook of MRI Pulse Sequences, Elsevier Academic Press, Burlington, 2004.
[22] T. Kitayama, K. Hatada, NMR Spectroscopy of Polymers, Springer, Verlag, Berlin, 2004.
[23] J.L. Koenig, Spectroscopy of Polymers, American Chemical Society, Washington, 1992.
[24] B. Widemann, K.H. Dusel, J. Eschl, Investigation into the influence of material and process on part distortion, Rapid Prototyp. J. 1 (1995) 17–22.
[25] M. Vatani, F. Barazandeh, A. Rahimi, A.S. Nezhad, Distortion modeling of SL parts by classical lamination theory, Rapid Prototyp. J. 18 (2012) 188–193.
[26] M. Simonelli, Y.Y. Tse, C. Tuck, Effect of the build orientation on the mechanical properties and fracture modes of SLM Ti-6Al-4V, Mater. Sci. Eng. A 616 (2014) 1–11.
[27] R.D. Goodridge, R.J.M. Hague, C.J. Tuck, Effect of long-term ageing on the tensile properties of a polyamide 12 laser sintering material, Polym. Test. 29 (2010) 483–493.